1D and 3D supramolecular structures exhibiting weak ferromagnetism in three Cu(II) complexes based on malonato and di-alkyl-2,2'-bipyridines

Jonathan Jaramillo-García, Antonio Téllez-López, Rogelio Martínez-Domínguez, Raul A. Morales-Luckie, Diego Martínez-Otero, Víctor Sánchez-Mendieta & Roberto Escudero

Taylor & Francis
Taylor & Francis Group

1D and 3D supramolecular structures exhibiting weak ferromagnetism in three Cu(II) complexes based on malonato and di-alkyl-2,2'-bipyridines

Jonathan Jaramillo-García[a], Antonio Téllez-López[a], Rogelio Martínez-Domínguez[a], Raul A. Morales-Luckie[b], Diego Martínez-Otero[b], Víctor Sánchez-Mendieta[a] and Roberto Escudero[c]

[a]Facultad de Química, Universidad Autónoma del Estado de México, Toluca, Mexico; [b]Centro Conjunto de Investigación en Química Sustentable UAEM-UNAM, Toluca, Mexico; [c]Instituto de Investigaciones en Materiales, Universidad Nacional Autónoma de México, Distrito Federal, Mexico

ABSTRACT

Three new Cu(II) complexes composed of malonato (mal), methylmalonato (memal), 4,4'-di-tert-butyl-2,2'-bipyridine (tbpy) and 5,5'-dimethyl-2,2'-bipyridine (mebpy) ligands, $Cu(H_2O)(mal)(tbpy)$ (**1**), $Cu(H_2O)(memal)(tbpy)$ (**2**) and $Cu_4(H_2O)_4(memal)_4(mebpy)_4 \cdot 11H_2O$ (**3**) were synthesized by simple one-pot solution reactions at ambient conditions. Single-crystal X-ray diffraction analyses reveal that the Cu(II) ions exhibit a distorted five-coordinate square pyramidal geometry. These three complexes display supramolecular arrays due to hydrogen-bonding interactions. Complexes **1** and **2** show 1-D supramolecular structures; **1** forms a double-ion chain, unlike **2**, which only generates a single-ion chain. In **3**, there are two identical monomers in the asymmetric unit with $Z'' = 2$; its high number of noncoordinated water molecules, along with hydrogen-bonding interactions between aqua ligand and memal ligand, generate a supramolecular tetramer, which mimics to produce a 3-D supramolecular framework. Besides this fascinating and yet uncommon crystallographic phenomenon in **3**, the structural differences found in these complexes arise from the substituted groups in the malonato dianion and in the bipyridine ligands. These compounds exhibit weak ferromagnetic-exchange interactions.
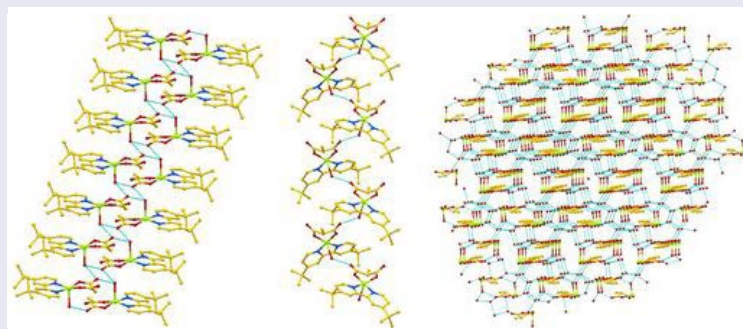
1. Introduction

Coordination chemistry has grown due to numerous different methodologies to synthesize coordination compounds [1], important properties and applications found in this class of compounds [2].

Selection of the metal ion and the ligand or ligands are essential in the formation of desired coordination compounds. Coordination geometry of the central ion, the structure and the binding mode of the ligand (monodentate, bidentate, bridging or chelating) and the reaction conditions can influence the final chemical structure of a coordination compound [3].

Several strategies have been developed to synthesize bivalent-transition metal complexes containing nitrogen and oxygen donor ligands [4]. Based on our previous studies of coordination polymers [5–7], constructing coordination complexes and polymers, from carboxylates and nitrogen-containing mixed ligands, has become our current interest. Among the most used bridging ligands for transition metal ions are dicarboxylate ligands [8]. In particular, malonate has been extensively used for the formation of coordination complexes [9] and coordination polymers [10]. We selected this ion-bridging ligand due to its simple chemical structure and its dual chemical functionality, which allow it to generate complexes or polymers, depending on its coordination modes [11]. In addition, the use of the methylmalonate [12] was based on the possible steric effect, from the alkyl group, affecting the final chemical structure.

The use of 2,2'-bipyridine as ancillary ligand had become relevant in our previous structural studies on coordination polymers and complexes [13–15]; therefore, we decided to just vary the alkyl substituent on it in order to verify the influence of the steric hindrance on the complexes structures.

Supramolecular chemistry is all about interactions between molecules, how they can recognize each other, assemble and function on a molecular scale [16]. Self-assembly of small molecules, compounds or complexes is a process for synthesizing large structures. Crystal engineering refers to construction of crystal structures from organic and metal organic compounds using design principles that come from an understanding of the intermolecular interactions in the molecular solids [17]. However, self-assembly is sometimes accompanied by uncertainty, due to unpredictable interactions among metal centers and ligands, especially when weak forces (i.e. hydrogen bonding, π–π interactions) and/or solvents, such as water, are involved [18]. Sometimes, the result of this structural-prediction complexity is the existence of compounds with high Z' or Z'' crystal structures, where $Z' = Z$/M; M is the multiplicity of the general position and Z is the number of residues in the unit cell; Z'' denotes the number of crystallographic nonequivalent molecules [19]. It is relevant to keep contributing new insight into possible crystal structures.

As stated by Olivier Kahn, the heart of the molecular magnetism involves the design and synthesis of molecular assemblies with properties such as long-range magnetic ordering [20]. Consequently, molecular magnetism could be considered as a feature of supramolecular chemistry dealing with open-shell structural units, leading thus, to the study of physical properties (magnetism) of supramolecular systems having unpaired electrons in their structures.

In this work, we report the synthesis, crystal structures, supramolecular chemistry, spectroscopic (IR), thermal and magnetic properties of three Cu(II) complexes based on malonate (mal), methylmalonate (memal), 4,4'-di-tertbutyl-2,2'-bipyridine (tbpy) and 5,5'-dimethyl-2,2'-bipyridine (mebpy) ligands.

2. Experimental

2.1. Materials and instrumentation

All chemicals were of analytical grade, purchased commercially (Aldrich) and used without purification. Elemental analyses for C, H, and N were carried out for standard methods using a Vario Micro-Cube analyzer. IR spectra of the complexes were determined as KBr disks in an Avatar 360 FT-IR E.S.P. Nicolet spectrophotometer from 4000 to 400 cm^{-1}. TGA experiments were performed in STA 449 F3 Jupiter Netzsch equipment, under N$_2$ atmosphere, at a heating rate of 10 °C min^{-1}, from 20 to 560 °C, using aluminum crucibles. Magnetic characteristics of the three complexes were determined in a MPMS Quantum Design magnetometer with measurements performed at zero field cooling (ZFC) and field

cooling (FC) modes from 2 to 300 K and decreasing. The applied magnetic field was 100 Oe, and the total diamagnetic corrections were estimated using Pascal's constants as -260×10^{-6}, -250×10^{-6}, -300×10^{-6} cm^3 mol^{-1} for **1**, **2** and **3**, respectively.

2.2. Crystallographic analyses

Crystallographic data for **1**, **2**, and **3** were collected on a Bruker SMART APEX DUO three-circle diffractometer equipped with an Apex II CCD detector using MoKα ($\lambda = 0.71073$ Å, Incoatec IµS microsource and Helios optic monochromator) –173 °C [21]. Suitable crystals of **1**, **2**, and **3** were coated with hydrocarbon oil, picked up with a nylon loop, and immediately mounted in the cold nitrogen stream (−173 °C) of the diffractometer. The structures were solved by direct methods (SHELXS-97) [22] and refined by full-matrix least-squares on F^2 [22] using the shelXle GUI [23]. The hydrogens of C–H bonds were placed in idealized positions, whereas hydrogens from water molecules were localized from the difference electron density map, and their position was refined with U_{iso} tied to the oxygen with distance restraints. The disordered tert-butyl group in **1** was refined using geometry and distance restraints (SAME, SADI together with the restraints for the U_{ij} values (SIMU, DELU, RIGU) implemented in SHELXL [22], the occupancy of the majority part is a 94.1(3)%. Some hydrogen atoms of the water molecules in **3** present positional disorder and were refined using distance restraints at 0.84 Å (DFIX implemented in SHELXL [22]).

2.3. Synthesis of complexes

2.3.1. Cu(H₂O)(mal)(tbpy) (1)
To a solution of Cu(CO$_3$)·Cu(OH)$_2$ (0.4442 g, 2.0 mmol) in hot deionized water (20 mL), malonic acid (0.1977 g, 1.9 mmol) was added, while stirring, and a dark blue solution was obtained. Then, it was filtered and condensed to 14 mL. To this solution, 4,4'-di-tert-butyl-2,2'-bipyridine (0.1006 g, 0.37 mmol) in 14 mL of methanol was added. After one week, dark blue crystalline needles were obtained, filtered, washed with a 50:50 deionized water-methanol solution and air-dried. Yield: 52% based on metal precursor. Anal. Calcd for C$_{21}$H$_{28}$CuN$_2$O$_5$: C, 55.80; H, 6.24; N, 6.19%. Found: C, 55.36; H, 6.23; N, 6.16%. IR (cm^{-1}): 3405 (s, br), 3239 (m), 3108 (w), 2958 (s), 1627 (vs), 1589 (s), 1415 (s), 1299 (m), 1253 (m), 1195 (w), 1145 (w), 1022 (m), 937 (m), 894 (m), 844 (m), 713 (m), 605(m), 551 (w), 454 (w).

2.3.2. Cu(H₂O)(memal)(tbpy) (2)
To a solution of Cu(CO$_3$)·Cu(OH)$_2$ (0.0590 g, 0.5 mmol) in hot deionized water (20 mL), methylmalonic acid (0.1105 g, 0.5 mmol) was added, while stirring, and a dark blue solution was obtained, which was filtered. To this filtrate, 4,4'-di-tert-butyl-2,2'-bipyridine (0.1342 g, 0.5 mmol) in 20 mL of methanol was added. After five days, large dark blue crystalline needles were obtained, filtered, washed with a 50:50 deionized water/methanol solution and air-dried. Yield: 57% based on metal precursor. Anal. Calcd for C$_{22}$H$_{30}$CuN$_2$O$_5$: C, 56.69; H, 6.48; N, 6.01%. Found: C, 56.58; H, 6.42; N, 6.02%. IR (cm^{-1}): 3668 (s, sh), 3298 (s, br), 3062 (s, br), 2966 (s), 2870 (w), 1643 (vs), 1550 (m), 1400 (s), 1269 (s), 1207 (w), 1121 (m, sh), 1022 (m), 937 (m), 894 (vm), 844 (m), 717 (m), 605(vm), 551 (m), 428 (m).

2.3.3. Cu₄(H₂O)₄(memal)₄(mebpy)₄·11H₂O (3)
To a solution of Cu(CO$_3$)·Cu(OH)$_2$ (0.0590 g, 0.5 mmol) in hot deionized water (20 mL), methylmalonic acid (0.1105 g, 0.5 mmol) was added, while stirring, and a dark blue solution was obtained, which was filtered. To this filtrate, 5,5'-dimethyl-2,2'-bipyridine (0.0920 g, 0.5 mmol) in 20 mL of methanol was added. After four days, dark blue crystalline needles were obtained, filtered, washed with a 50:50 deionized water/methanol solution and air-dried. Yield: 61% based on metal precursor. Anal. Calcd for C$_{64}$H$_{94}$Cu$_4$N$_8$O$_{31}$: C, 44.54; H, 5.49; N, 6.49%. Found: C, 44.80; H, 5.43; N, 6.52%. IR (cm^{-1}): 3386 (s, br), 2993 (w), 2935 (w), 1624 (vs), 1585 (s), 1477 (m), 1450 (m), 1415 (s), 1322 (m), 1272 (m), 1230 (m), 1160 (m), 1116(m), 1051 (m), 920 (w), 841 (m), 726 (m), 586 (w), 419 (m).

Table 1. Crystal data and structure refinement parameters for **1**–**3**.

	1	2	3
Empirical formula	$C_{21}H_{28}CuN_2O_5$	$C_{22}H_{30}CuN_2O_5$	$C_{64}H_{94}Cu_4N_8O_{31}$
Formula weight	451.99	466.02	1725.63
Temperature (K)		100(2)	
Wavelength (Å)		0.71073	
Crystal system		Monoclinic	Triclinic
Space group		P 21/c	P-1
a (Å)	5.98390(10)	13.2221(5)	12.1993(3)
b (Å)	18.2628(4)	10.1040(4)	12.9102(3)
c (Å)	20.0562(5)	15.8983(6)	14.1793(4)
α (°)	90	90	104.3371(5)
β (°)	98.5741(5)	94.7546	93.2901(5)
γ (°)	90	90	118.1182(4)
Volume (Å³)	2167.30(8)	2116.64(14)	1868.24(8)
Z	4	4	1
D_{Calcd} (Mg m⁻³)	1.385	1.462	1.534
Absorption coefficient (mm⁻¹)	1.041	1.068	1.214
F (0 0 0)	948	980	898
Crystal size (mm³)	$0.250 \times 0.212 \times 0.173$	$0.348 \times 0.297 \times 0.292$	$0.315 \times 0.226 \times 0.197$
Theta range for data collection (°)	2.230–25.686	1.927–25.349	1.905–25.350
Index ranges	-7 ≤ h ≤ 7, -22 ≤ k ≤ 22, -24 ≤ l ≤ 24	-15 ≤ h ≤ 15, -12 ≤ k ≤ 12, -19 ≤ l ≤ 19	-14 ≤ h ≤ 14, -15 ≤ k ≤ 15, -17 ≤ l ≤ 17
Reflections collected	20337	34863	47685
Independent reflections	4132 [R(int) = 0.0175]	3861 [R(int) = 0.0196]	6839 [R(int) = 0.0154]
Refinement method		Full-matrix least-squares on F^2	
Data/restraints/parameters	4132/75/305	3861/2/284	6839/34/556
Goodness-of-fit on F^2	1.048	1.008	1.040
Final R indices [$I > 2\sigma(I)$]	$R_1 = 0.0253$, $wR_2 = 0.0632$	$R_1 = 0.0232$, $wR_2 = 0.1057$	$R_1 = 0.0212$, $wR_2 = 0.0578$
R indices (all data)	$R_1 = 0.0264$, $wR_2 = 0.0638$	$R_1 = 0.0242$, $wR_2 = 0.1075$	$R_1 = 0.0217$, $wR_2 = 0.0581$
Largest diff. peakand hole e Å⁻³	0.758/−0.298	0.369/−0.578	0.461/−0.411

Table 2. Selected bond distances (Å) and angles (°) for **1**.

Bond lengths (Å)

Cu(1)–O(1)	1.9245(11)	Cu(1)–N(1)	2.0107(13)
Cu(1)–O(3)	1.9314(11)	Cu(1)–O(5)	2.2373(12)
Cu(1)–N(2)	1.9928(13)		

Angles ( )

O(1)–Cu(1)–O(3)	93.42(5)	N(2)–Cu(1)–N(1)	80.65(5)	
O(1)–Cu(1)–N(2)	169.01(5)	O(1)–Cu(1)–O(5)	96.58(5)	
O(3)–Cu(1)–N(2)	91.04(5)	O(3)–Cu(1)–O(5)	106.48(5)	
O(1)–Cu(1)–N(1)	91.37(5)	N(2)–Cu(1)–O(5)	91.76(5)	
O(3)–Cu(1)–N(1)	156.50(5)	N(1)–Cu(1)–O(5)	95.77(5)	
D–H⋯A	d(D–H)	d(H⋯A)	d(D⋯A)	<(DHA)
O(5)–H(5B)⋯O(2)#1	0.825(14)	2.009(15)	2.8185(17)	166.5(18)
O(5)–H(5A)⋯O(2)#2	0.833(14)	1.975(16)	2.7762(16)	161.2(18)

Notes: Symmetry transformations used to generate equivalent atoms: #1$x - 1$, y, z; #2$-x + 1$, $-y + 1$, $-z + 1$.

3. Results and discussion

Crystal data and refinement details for the complexes are given in table 1. Selected bond distances, angles, and hydrogen-bonding geometries of **1**, **2**, and **3** are listed in tables 2–4, respectively.

3.1. Crystal structures

The X-ray crystallographic analysis shows that **1** crystalizes in the monoclinic space group P 21/c. The molecular structure of **1** consists of one Cu(II), one mal, one tbpy and one coordinated water, as shown in figure 1. Cu(II) is five coordinate in a slightly distorted square pyramidal geometry, coordinated by

Table 3. Selected bond distances (Å) and angles (°) for **2**.

Bond lengths (Å)			
Cu(1)–O(1)	1.9229(9)	Cu(1)–N(2)	2.0011(10)
Cu(1)–O(3)	1.9354(9)	Cu(1)–O(5)	2.3304(9)
Cu(1)–N(1)	1.9992(10)		
Angles (°)			
O(1)–Cu(1)–O(3)	92.94(4)	O(3)–Cu(1)–N(2)	93.79(4)
O(1)–Cu(1)–N(1)	91.58(4)	N(1)–Cu(1)–N(2)	80.35(4)
O(3)–Cu(1)–N(1)	173.54(4)	O(1)–Cu(1)–O(5)	113.61(4)
O(1)–Cu(1)–N(2)	158.08(4)	O(3)–Cu(1)–O(5)	93.17(4)
N(1)–Cu(1)–O(5)	89.24(4)	N(2)–Cu(1)–O(5)	86.81(4)
D–H···A	d(D–H)	d(H···A)	d(D···A)	<(DHA)
O(5)–H(5B)···O(4)[#1]	0.840(8)	1.846(8)	2.6821(13)	173.7(16)

Notes: Symmetry transformations used to generate equivalent atoms: [#1]$-x + 1/2, y + 1/2, -z + 1/2$.

two carboxyl oxygens of mal, two nitrogens from the tbpy and the water. The basal plane is defined by O1, O3, N1, and N2, from the mal and tbpy ligands, respectively. The apical position is occupied by O5, from the coordinated water. Toward the apical water, the copper(II) deviates from the corresponding basal plane by 0.288 Å. The basal planes are tetrahedrally distorted with a τ value of 0.208 [$\tau = (169.01–156.50)/60 = 0.208$] [24]. Cu–O1 = 1.924(1) Å and Cu–O3 = 1.931(1) Å bond distances are as expected for similar malonate complexes [25]. Cu–N1 = 1.993(1) Å and Cu–N2 = 2.011(1) Å bond distances are in the normal range of related complexes [26]. Also, Cu–O5 = 2.237(1) Å bond distance is comparable to analogous compounds [27].

The crystal packing in **1** is stabilized mainly by hydrogen bonds. Adjacent complex units are connected by hydrogen bonds between non-coordinated carboxyl oxygen (O2) of mal and O5 of the coordinated water (figure 2, top). The up and down alternation of the complex configuration in the crystal lattice leads to a 1-D double-ion chain through hydrogen bonding (figure 2, bottom).

When mal is replaced by memal, **2** is obtained. The single-crystal X-ray analysis reveals that **2** crystallizes in the monoclinic space group P 21/n and the molecular structure of **2** consists of one Cu(II), one memal, one tbpy, and one coordinated water, as shown in figure 3. Cu(II) has a distorted square pyramidal coordination geometry, with a τ value of 0.257 [$\tau = (173.54–158.08)/60 = 0.257$] [24], formed by two carboxyl oxygens from memal, two nitrogens from tbpy and a coordinated water. O1, O3, N1, and N2 form the basal plane while O5 occupies the apical position. Toward this apical position, the Cu ion deviates from the corresponding basal plane by 0.231 Å. The Cu–N and Cu–O bond distances [Cu–O1 = 1.923(9), Cu–O3 = 1.935(9), Cu–N1 = 1.999(10), Cu–N2 = 2.001(10), and Cu–O5 = 2.330(9) Å] are similar to the corresponding ones in known Cu(II) complexes [25–28].

Crystal packing of **2** is achieved by intermolecular hydrogen bonds. Similarly to **1**, molecules of **2** are bridged by O–H···O hydrogen bonds coming from O5 of the coordinated water and the noncoordinated O4 from memal, respectively (figure 4, top), forming, thus, a zig-zag 1-D chain (figure 4, bottom). Inclusion of a methyl substituent in the malonato ligand precludes generating the double-ion chain exhibited in the intermolecular motif of **1**, due perhaps to steric hindrance, leading only to a 1-D chain supramolecular hydrogen-bonding structure in **2**.

By changing the 4,4'-ditert-butyl moiety, used in **1** and **2**, for 5,5'-dimethyl in the bipy ligand, and maintaining the memal dicarboxylic ligand as in **2**, the one-pot solution reaction of Cu(II), mebpy and memal produced **3**. The building units in the crystal structure for **3** are the hydrogen-bonded tetramer [$Cu_4(H_2O)_4(memal)_4(mebipy)_4$], and eleven lattice water molecules, as shown in figure 5 (bottom). Other similar dimer, trimer, tetramer, etc. Cu(II) complexes have been reported using malonato and bipyridine type ligands [29–32]. The asymmetric unit of **3** contains two Cu(II) ions, two memal, two mebpy, two aqua ligands, and the corresponding lattice water molecules (figure 5, top). The Cu(II) ions are each coordinated to one memal, one mebpy and a water to form a square pyramidal CuN_2O_3 chromophore with the water oxygen at the apical position. The equatorial Cu–N/O bond distances vary from 1.919(10) to 2.012(12) Å and axial Cu-O bond lengths of 2.292(11) and 2.254(11) Å were found for Cu1 and Cu2,

Table 4. Selected bond distances (Å) and angles (°) for **3**.

Bond lengths (Å)			
Cu(1)–O(5)	1.9192(10)	Cu(2)–O(1)	1.9187(10)
Cu(1)–O(7)	1.9241(10)	Cu(2)–O(3)	1.9378(10)
Cu(1)–N(4)	1.9999(13)	Cu(2)–N(1)	1.9933(12)
Cu(1)–N(3)	2.0060(12)	Cu(2)–N(2)	2.0119(12)
Cu(1)–O(15)	2.2924(11)	Cu(2)–O(9)	2.2543(11)
Angles (°)			
O(5)–Cu(1)–O(7)	92.24(4)	O(1)–Cu(2)–O(3)	91.57(4)
O(5)–Cu(1)–N(4)	171.13(5)	O(1)–Cu(2)–N(1)	91.98(5)
O(7)–Cu(1)–N(4)	92.03(5)	O(3)–Cu(2)–N(1)	165.48(5)
O(5)–Cu(1)–N(3)	92.71(5)	O(1)–Cu(2)–N(2)	163.99(5)
O(7)–Cu(1)–N(3)	164.57(5)	O(3)–Cu(2)–N(2)	91.80(5)
N(4)–Cu(1)–N(3)	81.24(5)	N(1)–Cu(2)–N(2)	81.10(5)
O(5)–Cu(1)–O(15)	94.97(4)	O(1)–Cu(2)–O(9)	100.92(4)
O(7)–Cu(1)–O(15)	101.65(4)	O(3)–Cu(2)–O(9)	95.24(4)
N(4)–Cu(1)–O(15)	91.78(5)	N(1)–Cu(2)–O(9)	97.90(4)
N(3)–Cu(1)–O(15)	92.47(4)	N(2)–Cu(2)–O(9)	94.35(4)

D–H···A	d(D–H)	d(H···A)	d(D···A)	<(DHA)
O(9)–H(9B)···O(11)	0.832(14)	1.892(15)	2.7185(16)	172.2(17)
O(9)–H(9A)···O(4)[#1]	0.838(14)	1.971(15)	2.7687(15)	158.8(17)
O(10)–H(10A)···O(1)[#2]	0.817(15)	2.59(2)	3.1867(16)	130.7(19)
O(10)–H(10A)···O(2)[#2]	0.817(15)	2.051(15)	2.8350(17)	161(2)
O(10)–H(10B)···O(11)	0.831(18)	1.862(19)	2.6764(18)	166(4)
O(11)–H(11D)···O(8)	0.854(14)	1.848(15)	2.6906(16)	168.3(19)
O(11)–H(11E)···O(16)[#1]	0.843(18)	1.916(18)	2.7501(17)	170(4)
O(11)–H(11F)···O(10)	0.845(18)	1.836(19)	2.6764(18)	173(4)
O(13)–H(13B)···O(14)	0.850(15)	1.901(15)	2.739(2)	168(2)
O(13)–H(13A)···O(12)	0.844(12)	1.968(13)	2.777(3)	160(2)
O(13)–H(13A)···O(12)[#3]	0.844(12)	1.896(16)	2.659(3)	149.6(19)
O(14)–H(14B)···O(3)[#4]	0.844(15)	2.012(15)	2.8532(16)	175(2)
O(14)–H(14A)···O(6)[#5]	0.851(15)	1.934(15)	2.7747(16)	169(2)
O(15)–H(15A)···O(13)	0.818(15)	1.891(16)	2.6992(17)	169(2)
O(15)–H(15B)···O(6)[#5]	0.847(15)	1.958(16)	2.7729(15)	161.1(19)
O(16)–H(16D)···O(4)	0.852(14)	1.986(15)	2.8175(16)	164.8(19)
O(16)–H(16E)···O(11)[#1]	0.854(18)	1.93(2)	2.7501(17)	161(3)
O(16)–H(16F)···O(13)[#6]	0.892(16)	1.869(17)	2.7293(19)	161(2)

Notes: Symmetry transformations used to generate equivalent atoms: [#1]−x+2, −y+2, −z+2; [#2]−x+1, −y+1, −z+2; [#3]−x+2, −y+2, −z+3; [#4]x, y, z+1; [#5]−x+2, −y+1, −z+3; [#6]x, y, z−1.
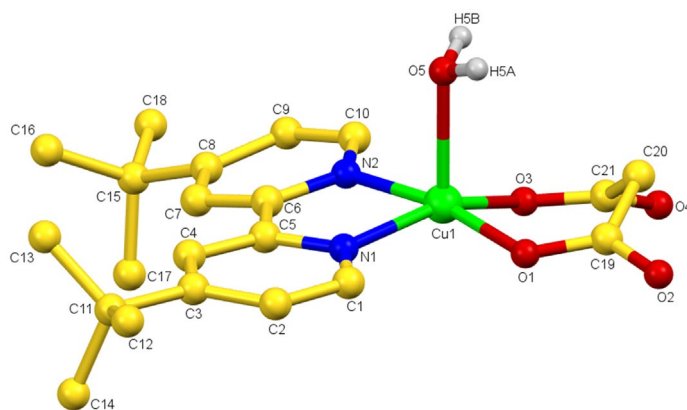
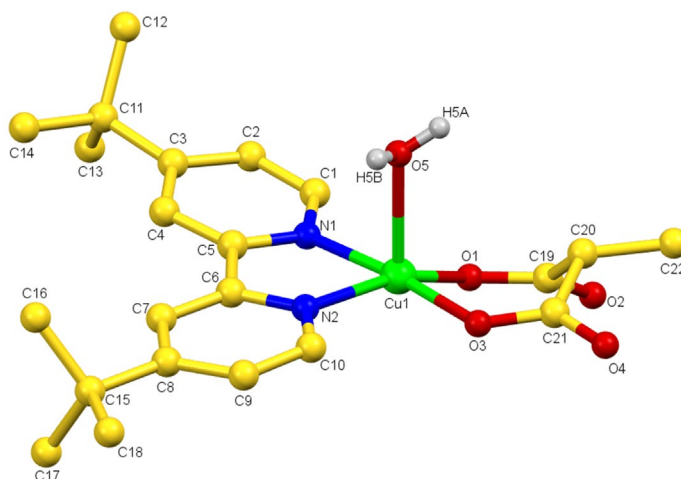**Figure 1.** Molecular structure of Cu(H$_2$O)(mal)(tbpy) (**1**).
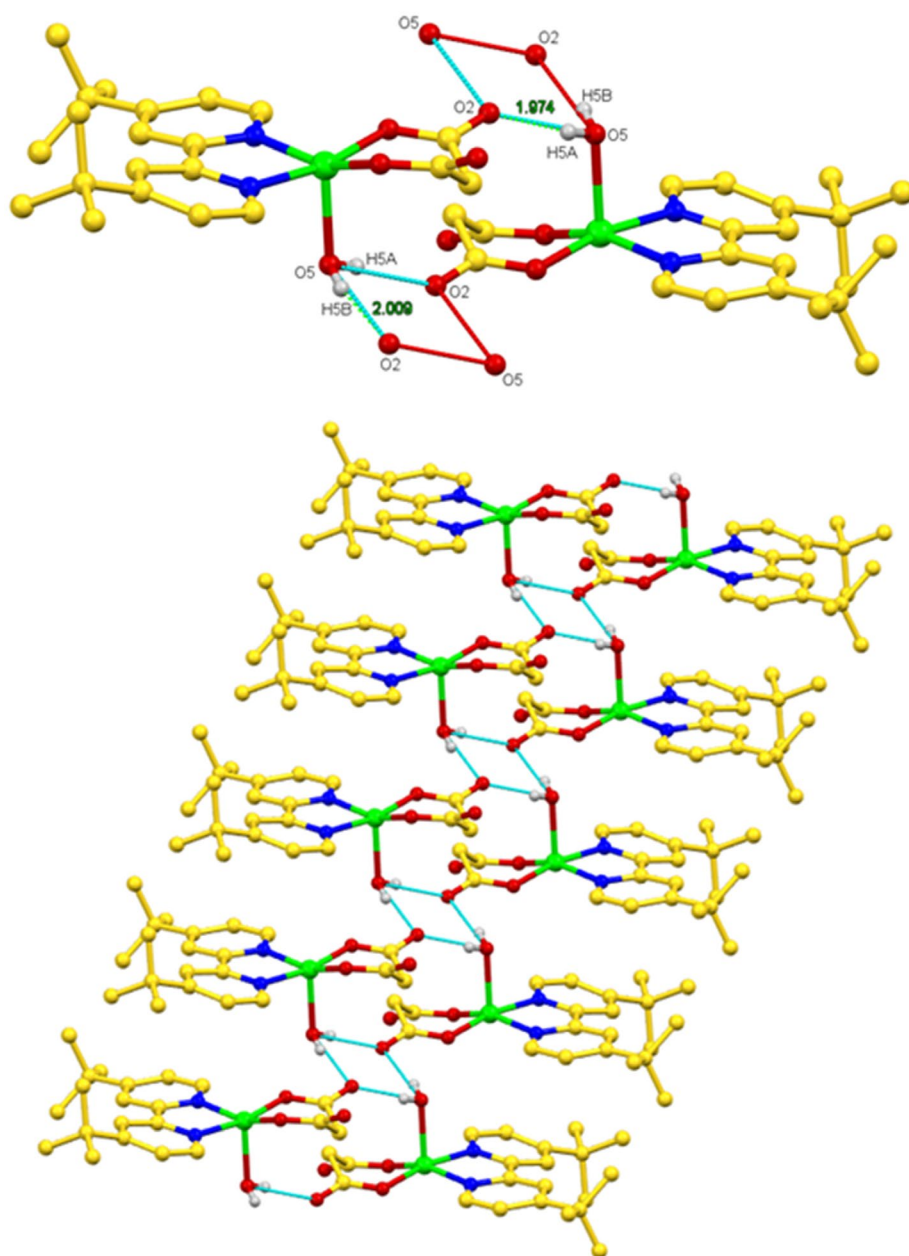
Figure 2. Hydrogen-bonding main connections in **1** (top); supramolecular 1-D double-ion chain of **1** formed by hydrogen-bonding interactions (bottom); views looking perpendicular to the *ab* plane. Most hydrogens are omitted for clarity.

respectively (table 4). The basal planes are tetrahedrally distorted and the τ values [24] are 0.109 and 0.025 for Cu1 and Cu2, respectively. Cu1 and Cu2 are displaced by 0.206 and 0.261 Å, respectively, from the corresponding basal plane toward the apical position.

Two [Cu(H$_2$O)(memal)(mebpy)] complex molecules are associated into a dinuclear [Cu$_2$(H$_2$O)$_2$(memal)$_2$(mebipy)$_2$] complex throughout O–H⋯O hydrogen bonding from O4 to O8 of the memal ligands, and O9 and O15 of the corresponding aqua ligands. In addition, O10, O11, O13, O14, and O16 of lattice water molecules generate hydrogen bonds (figure 5, top). The resulting dimers are

Figure 3. Molecular structure of Cu(H$_2$O)(memal)(tbpy) (**2**).

each hydrogen bonded to other two [Cu(H$_2$O)(memal)(mebpy)] complexes to generate a supramolecular tetramer [Cu$_4$(H$_2$O)$_4$(memal)$_4$(mebpy)$_4$], which is the basis for the crystallographic lattice in **3** (figure 5, bottom). In comparison to those structures where the kinetic and thermodynamic forms are the same, this type of asymmetrical units with more than one molecule (Z′ > 1) are still considered as rarities in crystallography, since crystal structures with these characteristics are rather small in number [18]. These high Z′ structures signify high energy minima in the crystallization path towards the final thermodynamic crystal. Sometimes the process leading to the formation of these crystals is referred to as "frozen" or interrupted crystallization. Even more, it has been identified that supramolecular synthons play an important role in obtaining this type of crystals, as could have been in the crystallization process of **3** with Z″ = 2 [18, 32]. Thus, these tetramers are stabilized by weak intermolecular hydrogen bonds, due primarily to the lattice water molecules surrounding the complexes. In this array, Cu1 and Cu2 ions generate alternate parallel double-ion 1-D chains, which are interconnected to each other to form a 2-D network, which is then connected, principally, by lattice water molecules via hydrogen bonding, leading to the formation of a 3-D supramolecular structure in **3** (figure 6).

Hence, according to the dissimilar supramolecular arrays obtained for **1**, **2**, and **3**, the crystal structure differences in these complexes may be attributed to variations in the substituted groups in both lignads, the malonato dianion, and the bipyridine. Consequently, while **1** can achieve a double-ion 1-D chain supramolecular structure, **2** can only form a single-ion 1-D chain, by just adding a methyl group to C20 of malonate (figures 1–4). Steric interferences in the crystal can be acting in this case, avoiding further hydrogen-bonding interactions. For **3**, elimination of the steric hindrance from tert-butyl groups by using mebipy in the 5,5′ positions encourages formation of a supramolecular tetranuclear compound, and, additionally to this, the occurrence of several lattice water molecules in **3** promotes the 3-D supramolecular array (figures 5 and 6).

3.2. Thermal analyses

To examine the thermal stability of the three compounds, thermal analyses were performed for **1**, **2**, and **3** between 20 and 560 °C (figure 7).

Complexes **1** and **2** exhibit two decomposition stages. The first major weight loss (18.00%) for **1** occurs between 195 and 240 °C and the second one, with a weight loss of 58.59% of the initial weight, takes place approximately between 240 and 310 °C. Likewise, for **2** the first weight loss (20.55%) appears between 179 and 222 °C and the second, with a weight loss of 59.59%, happens between 227 and 300 °C.
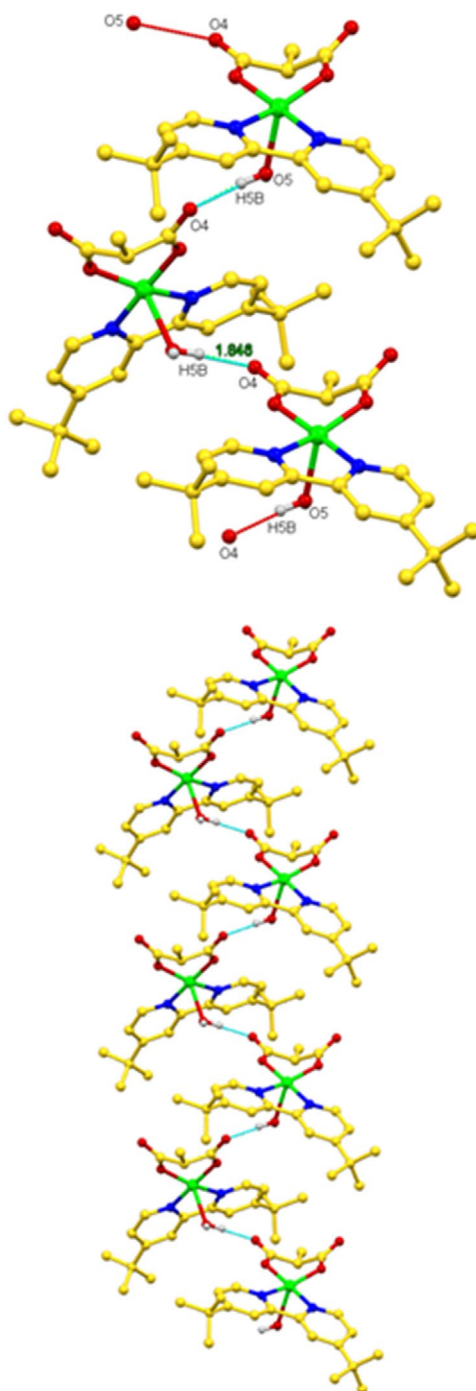
Figure 4. Hydrogen-bonding main connections in **2** (top); supramolecular 1-D zig-zag chain of **2** formed by hydrogen-bonding interactions (bottom); views looking perpendicular to the *ab* plane. Most hydrogens are omitted for clarity.

In both complexes, the first decomposition stage can be attributed to combustion of mal (Calcd 22.50%) and memal (Calcd 25.34%) ligands for **1** and **2**, respectively; the second one can be assigned to the tbpy combustion: Calcd 59.38% for **1** and 57.59% for **2**. Complex **3** exhibits three stages of decomposition.
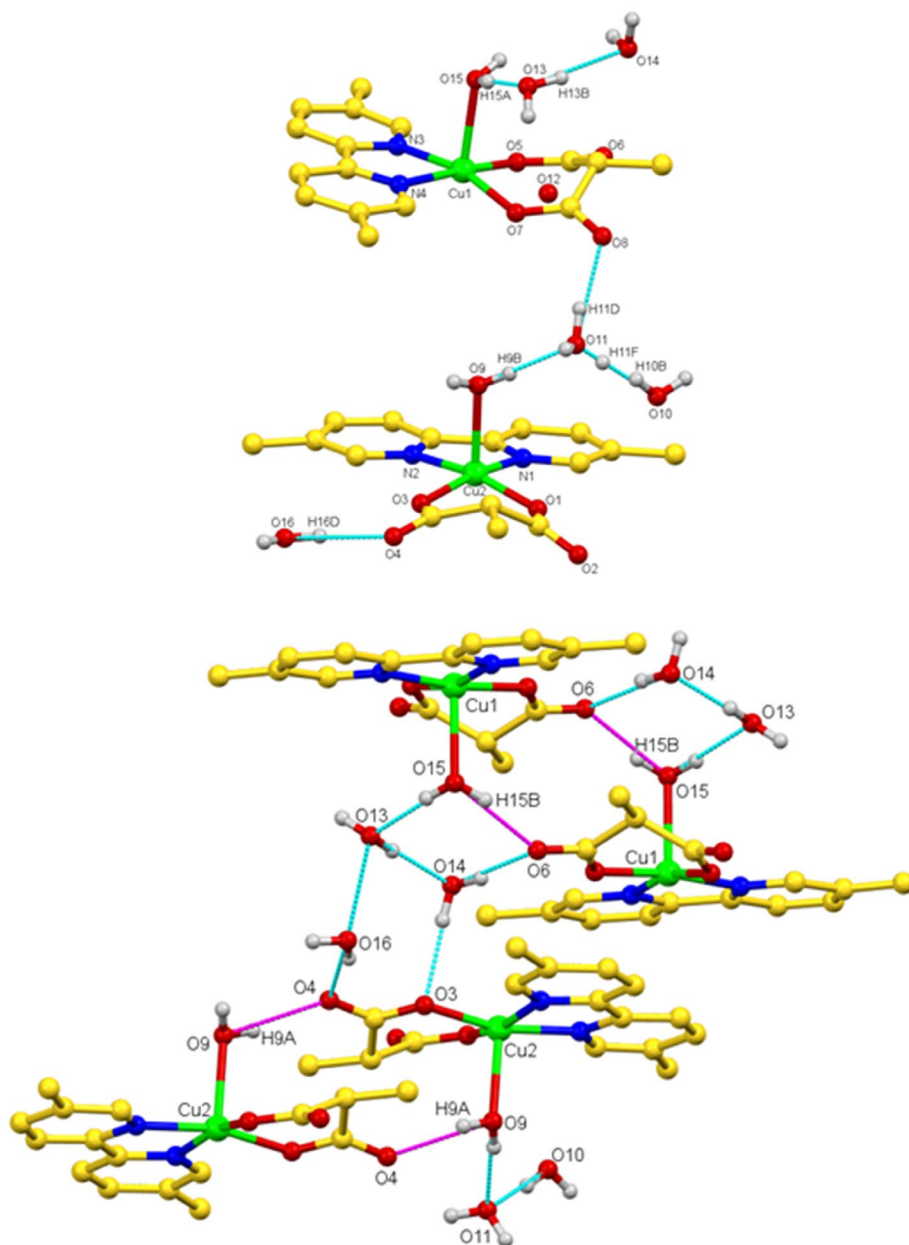
Figure 5. Hydrogen-bonding main connections in the dinuclear asymmetric structure of **3**; view looking perpendicular to the *ab* plane (top). Molecular structure of $Cu_4(H_2O)_4(memal)_4(mebpy)_4 \cdot 11H_2O$ (**3**) and hydrogen bonding motif. View looking perpendicular to the *bc* plane (bottom). Most hydrogens are omitted for clarity.

The first is credited to loss of 11 lattice water molecules (Calcd 11.02%), from 86 to 115 °C, with a weight loss of 9.52%. The second and third stages are not that well defined; the second stage, between 202 and 224 °C, has an approximate weight loss of 18.27%, corresponding, perhaps, to the combustion of four memal ligands, and the third stage from 227 to 293 °C can be attributable to the combustion of four mebpy ligands (Calcd 42.68%) with an experimental weight loss of 40.40%. TGA results for **3** also prove the tetramer character of this compound.
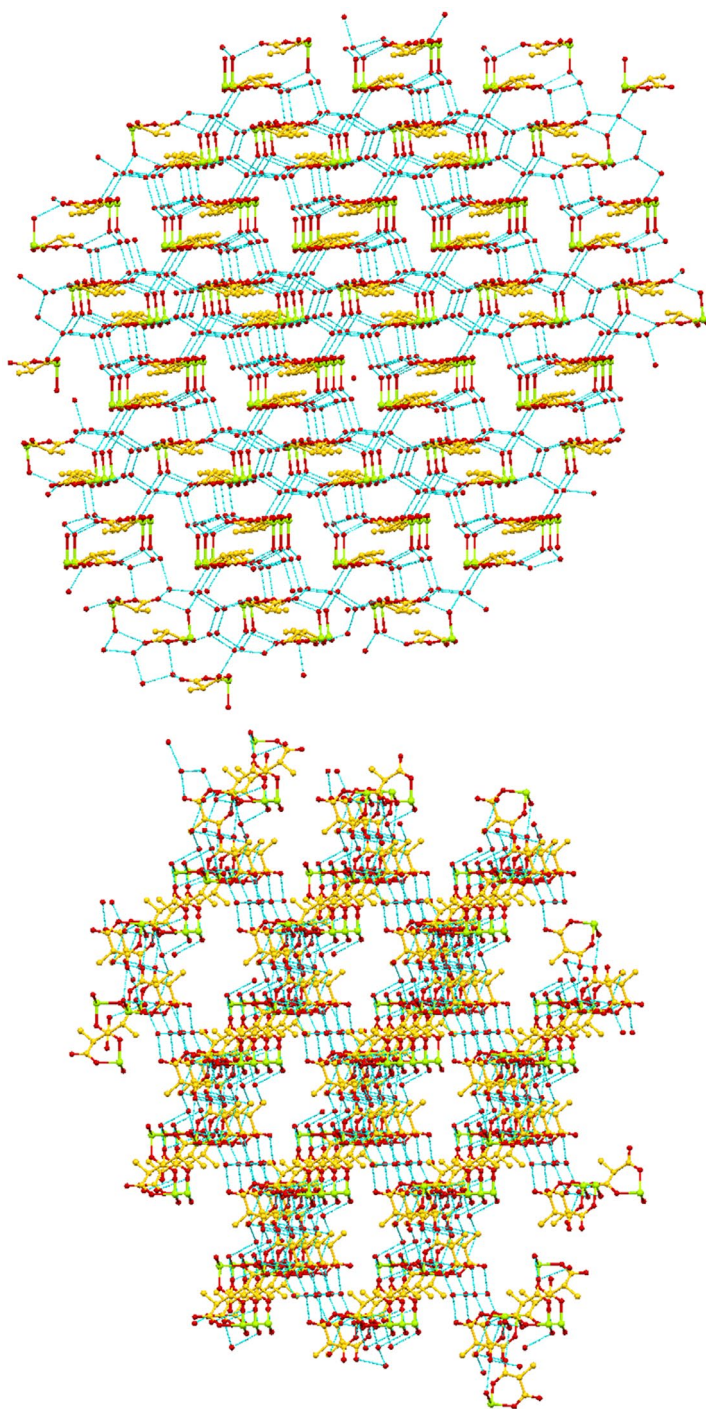
Figure 6. 3-D supramolecular structure of **3** formed by hydrogen bonding interactions; view looking almost down the *a* axis (top); view looking almost down the *c* axis (bottom). Hydrogens and mebpy ligands are omitted for clarity.
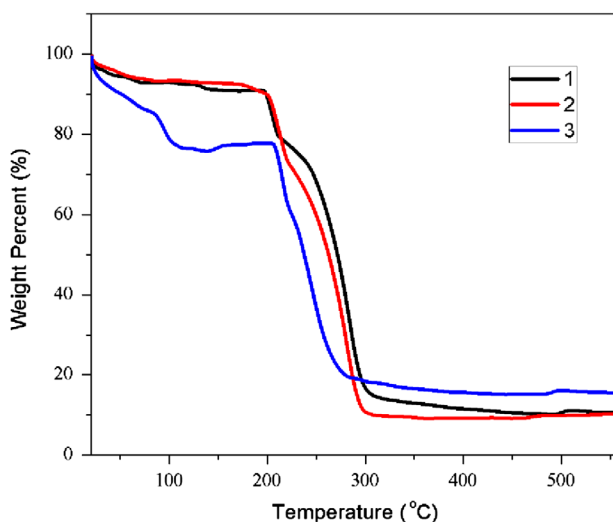
Figure 7. TGA plots for **1**, **2** and **3**.

3.3. Magnetic properties

The calculated magnetic susceptibility (χ), in terms of cm^3 mol^{-1}, *versus* temperature for **1**, **2**, and **3**, can be seen in figure 8; magnetic susceptibility was determined at ZFC and FC modes, from 2 to 300 K and decreasing. χT values at room temperature are 0.48, 0.45, and 1.76 cm^3 mol^{-1} K for **1**, **2**, and **3**, respectively. These are close to the values expected for one (**1** and **2**) and four (**3**) magnetically isolated Cu^{2+} ions.

The function used for the fitting of the χ *versus* T plots was:

$$\chi(T) = -\alpha T + C/\{T(1 + (\theta/T)^2 - (\theta/T)^3) - \theta)\} + X_o$$

with $\theta = 0.90$, 0.97, and 2.00 K for **1**, **2**, and **3**, respectively, and values for $C = 0.31$, 0.32, and 2.00 cm^3 K mol^{-1} for **1**, **2**, and **3**, respectively; $aT = -2e^{-7}T$ cm^3 mol^{-1}. This number is a phenomenological value, used to set the level of the constant susceptibility background. The term X_o is almost a constant value that changes very slowly; its values are 0.004 to 0.0073 cm^3 mol^{-1} for these compounds. This term is necessary because it allows a suitable physical interpretation of C and θ. The introduced theoretical model was deduced by Opechowski and Li [33, 34]. This model deals with short-range magnetic order included in the term $zJ/2kT$ which can be associated with the θ value of the Curie–Weiss model when $s = 1/2$, since $\theta = 2zJs(s + 1)/3\ k$ [33–35]. In fact, the values obtained are well appropriated for the characterization of these complexes with $s = 1/2$ for **1** and **2**, and $s = 1$ for **3**. These fitting values are consistent with the presence of weak ferromagnetism in these complexes, specifically in their supramolecular structures, although they reveal mainly short-range magnetic ordering. Plots of χ^{-1} *versus* T for **1**, **2**, and **3**, exhibiting excellent fitting, have been included as supplementary material (figure S1). It is quite important to mention that the Curie–Weiss law was at first used, but was discarded for the extreme values obtained for the Curie–Weiss temperature, and the fittings were not good, particularly at low temperatures. It is also worth mentioning that we tried to use the Bonner–Fisher model to describe the magnetic susceptibility; however, the results were not good and the parameter used quite unphysical. The obtained Curie–Weiss temperatures can be used to estimate the values of the magnetic interaction by using the mean-field expression: $\theta = zJs(s + 1)/3\ k$ [32–35], where z is the number of nearest-neighbor ions, J is the exchange integral, s is the spin, and k the Boltzmann constant. The estimated values are: $zJ = 2.50$, 2.69, and 2.08 cm^{-1} for **1**, **2**, and **3**, respectively, confirming the ferromagnetic coupling occurring in these compounds. In addition, according to their hydrogen-bonding supramolecular structures, z for
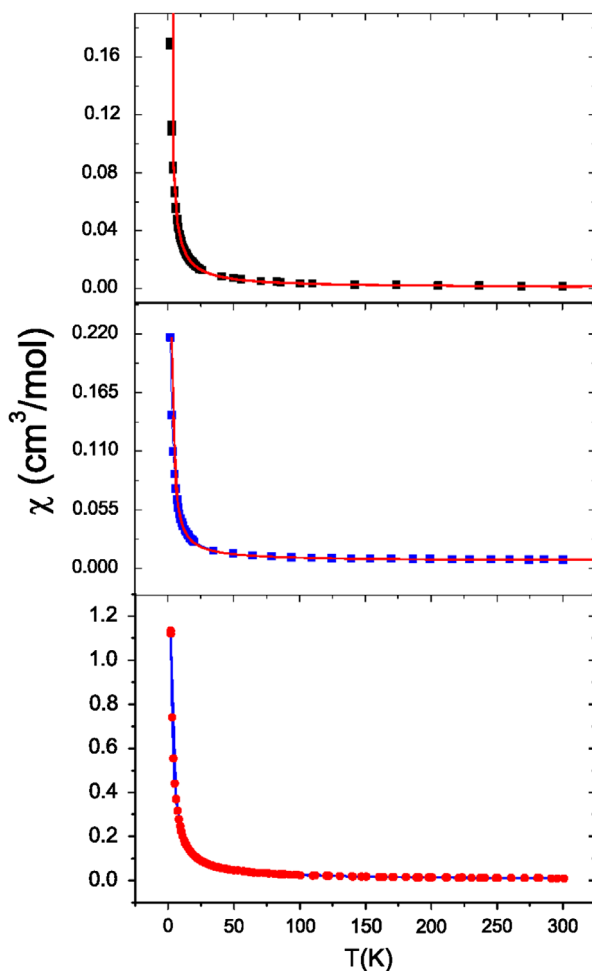
Figure 8. χ *vs.* T plots for **1** (top), **2** (middle), and **3** (bottom).

1, **2**, and **3** are 3 (double-ion chain), 2 (single-ion chain) and 3 (tetrameric unit), respectively (figures 2, 4, and 5). For **3**, the θ value used to calculate zJ corresponds to a supramolecular dimer with $s = 1$, as mentioned previously.

The main magnetic-exchange pathway in the three complexes appears to be the strong hydrogen-binding interactions occurring, mainly, through the connections involving the coordinated water and one of the oxygens in the carboxylate moiety of malonato ligand, belonging to a neighboring complex molecule, [Cu–Ow–H···O–C–O–Cu] (figures 2, 4, and 5). Distances between nearest neighboring Cu ions in **1** and **2**, through this kind of magnetic exchange pathway, are [Cu1–O5–H5B···O2–C19–O1–Cu1] = 9.503 Å and [Cu1–O5–H5B···O4–C21–O3–Cu1] = 9.465 Å, respectively. For **3**, two almost identical pathways could be devised, both involving intermolecular hydrogen bridging. One includes the connection of Cu1 ions [Cu1–O15–H15B···O6–C29–O5–Cu1] = 9.505 Å and the other embraces the connections between Cu2 ions [Cu2–O9–H9A···O4–C15–O3–Cu2] = 9.484 Å (figure 5 and figure S2, magenta dashed lines). These intermolecular interactions in **3** dinuclear clusters are similar to those occurring in **1** (figure 2). Furthermore, in **3**, additional exchange corridors could be involved, which include noncoordinated water molecules, such as the one that connects the two dinuclear units [Cu2–O9–H9B···O11–H11D···O8–C31–O7–Cu1] = 12.100 Å, to generate the supramolecular tetranuclear unit cell (figure 5 and figure S2).

Furthermore, one possibility to explain our results by using $s = 1$ in **3** is that the low energy excitations are dominated by the single triplet state of the tetramer; thus, the low-energy physics can be described by a spin-dimer system, and therefore, the possible intra (tetramer) and inter (among tetramers) exchange interactions occurring in **3** may be considered very small, almost zero, and not affecting the value of the J parameter, reason to use only a kind of Bonner–Fisher model, implying, thus, a Cu(II) dimer trough hydrogen bonding interactions. Accordingly, based on the very good fitting results from the short-range magnetic interaction model applied to the magnetic susceptibility measurements (figures 8 and S1), and because of the long distances among Cu ions between tetramers in the 3-D supramolecular structure of **3**, which have to go through at least one hydrogen-bridging interaction involving noncoordinated water molecules, we decided to include just one J parameter in the magnetic properties analysis of **3**, as well as in the other complexes. In general, the inter and intraexchange interactions experimentally are situated at $T \sim J/k$, when a maximum is observed. In our experiment, the magnetic susceptibility curve is a smooth function of temperature, there is no maximum, and therefore, possible inter and intraexchange interactions could be very small, and perhaps occurring at very low temperatures.

Malonate has been extensively studied regarding its role as a magnetic-exchange passageway in Cu(II) complexes, polynuclear compounds and coordination polymers [36–38]. In most cases, malonato ligand promotes ferromagnetic coupling. In previous studies about the magnetostructural correlations of malonato-based Cu(II) complexes and extended systems [37–40], it was concluded that the parameter that rules, primarily, the magnetic interaction between metal ions is the relative position of the carboxylato bridge of the malonate ligand related to the Cu(II) ions: equatorial-equatorial (strong interaction), equatorial-apical (weak interaction) and apical-apical (negligible interaction). According to their supramolecular structures, **1**, **2**, and **3** form chains with a regular alternation of the corresponding complex units, which are linked as a bidentate (η^5-chelation) + monodentate (**1**), bidentate (η^5-chelation) + mono-dentate (**2**), bidentate (η^5-chelation) + bis(monodentate) (**3**) ligand through two carboxylate oxygens of the malonate, via hydrogen-bonding interactions, with the antisyn coordination mode (figures 2, 4, and 5), which correspond to the equatorial-apical carboxylate bridge in the solid-state supramolecular structures. Thus, the magnetostructural correlations of the three analyzed complexes confirm the ferromagnetic-exchange coupling found. A survey of the J values for some carboxylate-bridged Cu(II) malonate complexes has been published recently [32]. In that study, most of these types of compounds have ferromagnetic-exchange couplings, particularly those with antisyn malonato coordination. Antiferromagnetic-exchange pathway via malonato has also been reported for a tetranuclear Cu(II) malonate complex leading to a 2-D supramolecular structure [32] with certain structural similarities to **3**. Though in our case, complex **3** possesses a more intricate hydrogen-bonding network due to the presence of 11 noncoordinated waters in its solid-state 3-D supramolecular structure. Hydrogen-bond magnetic interactions have been reported previously for other Cu(II) complexes and polymers, including malonate or its derivatives and have been described exhibiting both antiferromagnetic behavior [32, 41, 42] and ferromagnetic exchange [26, 29, 40, 43–45]. Therefore, according to the above mentioned, the obtained values for the exchange coupling constant (*vide supra*) for the three complexes are in agreement with those recently reported for Cu(II) complexes having hydrogen bonding or other intermolecular interactions [46–51].

Thence, **1**, **2**, and **3** exhibit weak ferromagnetic exchange interactions between the Cu(II) centers throughout the main hydrogen bond interactions occurring in supramolecular arrays, in agreement with the fitted magnetic data showing only one significant exchange pathway [46]. Therefore, it is still important, from the point of view of the magnetochemistry, to keep investigating this special coupling via hydrogen-bond interactions in supramolecular frameworks of this kind of complexes.

4. Conclusion

Three Cu(II) complexes of malonate and di-alkyl-2,2′-bipyridines have been prepared by one-pot assembly reactions at ambient conditions and structurally characterized. Cu(II) ions exhibit a distorted

five-coordinate square pyramidal geometry. These complexes display supramolecular arrays due to strong hydrogen-bonding interactions. Due to structural changes in the malonato ligand, **1** displays a double-ion ID chain and **2** exhibits a single-ion 1-D chain. In **3**, a rare kinetically favored crystal with $Z'' = 2$ was obtained and, as a consequence, a 3-D supramolecular framework is achieved owing to supramolecular hydrogen-bonding tetranuclear building unit and the presence of several lattice water molecules. The antisyn coordination mode of the malonato ligand, alongside strong hydrogen bonds, are responsible for the weak ferromagnetic-exchange interactions exhibited by the three complexes in their solid-state supramolecular arrays. Our work, thus, further demonstrates that magnetic-exchange pathways can be mediated by diamagnetic atoms, such as those involved in hydrogen-bonding supramolecular interactions.

Supplementary material

CCDC-1023592, 1023593 and 1023594 contain supplementary crystallographic data for **1**, **2**, and **3**, respectively. These data can be obtained free of charge via http://www.ccdc.cam.ac.uk/conts/retrieving/html, or from the Cambridge Crystallographic Data Center (CCDC), 12 Union Road, Cambridge CB2 1EZ, UK [Fax: (+44) 1223-336-033; E-mail: deposit@cdc.cam.ac.uk].

Acknowledgements

Disclosure statement

No potential conflict of interest was reported by the authors.

Funding

References

[1] E.C. Constable, C.E. Housecroft. *Chem. Soc. Rev.*, **42**, 1429 (2013).
[2] Z. Ma, B. Moulton. *Coord. Chem. Rev.*, **255**, 1623 (2011).
[3] Y.Y. Yang, W. Guo, M. Du. *Inorg. Chem. Commun.*, **13**, 1195 (2010).
[4] M. Du, C.-P. Li, C.-S. Liu, S.-M. Fang. *Coord. Chem. Rev.*, **257**, 1282 (2013).
[5] V. Sánchez, A. Storr, R.C. Thompson. *Can. J. Chem.*, **80**, 133 (2002).
[6] S.J. Rettig, V. Sanchez, A. Storr, R.C. Thompson, J. Trotter. *J. Chem. Soc., Dalton Trans.*, 3931 (2000).
[7] S.J. Rettig, V. Sánchez, A. Storr, R.C. Thompson, J. Trotter. *Inorg. Chem.*, **38**, 5920 (1999).
[8] D. Curiel, M. Más-Montoya, G. Sánchez. *Coord. Chem. Rev.*, **284**, 19 (2014).
[9] S.R. Choudhury, H.M. Lee, T.-H. Hsiao, E. Colacio, A.D. Jana, S. Mukhopadhyay. *J. Mol. Struct.*, **967**, 131 (2010).
[10] Y. Rodríguez-Martín, M. Hernández-Molina, F.S. Delgado, J. Pasán, C. Ruiz-Pérez, J. Sanchiz, F. Lloret, M. Julve. *Cryst. Eng. Comm.*, **4**, 522 (2002).
[11] X.-J. Zhao, Z.-H. Zhang, Y. Wang, M. Du. *Inorg. Chim. Acta*, **360**, 1921 (2007).
[12] J. Pasán, J. Sanchiz, L. Cañadillas-Delgado, O. Fabelo, M. Déniz, F. Lloret, M. Julve, C. Ruiz-Pérez. *Polyhedron*, **28**, 1802 (2009).
[13] B.O. Patrick, W.M. Reiff, V. Sánchez, A. Storr, R.C. Thompson. *Inorg. Chem.*, **43**, 2330 (2004).
[14] A. Téllez-López, J. Jaramillo-García, R. Martínez-Domínguez, R.A. Morales-Luckie, M.A. Camacho-Lopez, R. Escudero, V. Sánchez-Mendieta. *Polyhedron*, **100**, 373 (2015).
[15] R.D. Hancock. *Chem. Soc. Rev.*, **42**, 1500 (2013).
[16] J.M. Lehn. *Supramolecular Chemistry*., VCH, Weinheim (1995).
[17] G.R. Desiraju, J.J. Vittal, A. Ramanan. *Crystal Engineering-A Text Book*, IISc Press and World Scientific, Singapore (2011).
[18] D. Das, R. Banerjee, R. Mondal, J.A.K. Howard, R. Boese, G.R. Desiraju. *Chem. Commun.*, 555 (2006).

[19] B.P. van Eijck, J. Kroon. *Acta Cryst.*, **B56**, 535 (2000) (erratum: ibid, 745).
[20] O. Kahn. *Magnetism: A Supramolecular Function*, NATO Science Series C, Vol 484, Springer, Netherlands (1996).
[21] *APEX 2 software suite*, Bruker AXS Inc., Madison, Wisconsin, USA (2012).
[22] SHELX, G.M. Sheldrick. *Acta Crystallogr., Sect. A*, **64**, 112 (2008).
[23] shelXle, C.B. Hübschle, G.M. Sheldrick, B. Dittrich. *J. Appl. Cryst.*, 44, 1281 (2011).
[24] A.W. Addison, T.N. Rao, J. Reedijk, J. van Rijn, G.C. Verschoor. *J. Chem. Soc., Dalton Trans.*, 1349 (1984).
[25] G.-H. Cui, J.-R. Li, T.-L. Hu, X.-H. Bu. *J. Mol. Struct.*, **738**, 183 (2005).
[26] Y. Rodríguez-Martín, J. Sanchiz, C. Ruiz-Pérez, F. Lloret, M. Julve. *Inorg. Chim. Acta*, **326**, 20 (2001).
[27] H.-Y. Shen, W.-M. Bu, D.-Z. Liao, Z.-H. Jiang, S.-P. Yan, G.-L. Wang. *Inorg. Chem. Commun.*, **3**, 497 (2000).
[28] C. Gkioni, A.K. Boudalis, Y. Sanakis, C.P. Raptopoulou. *Polyhedron*, **26**, 2536 (2007).
[29] Y.-Q. Zheng, X.-S. Zhai, L. Jin, H.-L. Zhu, J.-L. Lin, W. Xu. *Polyhedron*, **68**, 324 (2014).
[30] C. Ruiz-Pérez, M. Hernández-Molina, P. Lorenzo-Luis, F. Lloret, J. Cano, M. Julve. *Inorg. Chem.*, **39**, 3845 (2000).
[31] Q.Z. Zhang, C.Z. Lu, W.B. Yang. *J. Coord. Chem.*, **58**, 1759 (2005).
[32] S.R. Choudhury, H.M. Lee, T.-H. Hsiao, E. Colacio, A.D. Jana, S. Mukhopadhyay. *J. Mol. Struct.*, **967**, 131 (2010).
[33] W. Opechowski. *Physica*, **4**, 715 (1937).
[34] Y.Y. Li. *Phys. Rev.*, **84**, 721 (1951).
[35] T. Nakano, M. Oda, C. Manabe, N. Momono, Y. Miura, M. Ido. *Phys. Rev.*, **49**, 16000 (1994).
[36] N. Shannon. *Eur. Phys. J. B*, **27**, 527 (2002).
[37] H. El Bakkali, A. Castiñeiras, I. García-Santos, J.M. González-Pérez, J. Niclós-Gutiérrez. *Cryst. Growth Des.*, **14**, 249 (2014).
[38] J. Pasán, F.S. Delgado, Y. Rodríguez-Martín, M. Hernández-Molina, C. Ruiz-Pérez, J. Sanchiz, F. Lloret, M. Julve. *Polyhedron*, **22**, 2143 (2003).
[39] C. Ruiz-Pérez, Y. Rodríguez-Martín, M. Hernández-Molina, F.S. Delgado, J. Pasán, J. Sanchiz, F. Lloret, M. Julve. *Polyhedron*, **22**, 2111 (2003).
[40] J. Pasán, J. Sanchiz, F. Lloret, M. Julve, C. Ruiz-Pérez. *Polyhedron*, **30**, 2451 (2011).
[41] C. Gkioni, A.K. Boudalis, Y. Sanakis, L. Leondiadis, V. Psycharis, C.P. Raptopoulou. *Polyhedron*, **27**, 2315 (2008).
[42] J. Costa, N.A.G. Bandeira, B. Le Guennic, V. Robert, P. Gamez, G. Chastanet, L. Ortiz-Frade, L.Gasque. *Inorg. Chem.*, 50, 5696 (2011).
[43] J. Pasán, J. Sanchiz, C. Ruiz-Pérez, F. Lloret, M. Julve. *Eur. J. Inorg. Chem.*, 4081 (2004).
[44] A. Das, B. Dey, A.D. Jana, J. Hemming, M. Helliwell, H.M. Lee, T.-H. Hsiao, E. Suresh, E. Colacio, S.R. Choudhury, S. Mukhopadhyay. *Polyhedron*, **29**, 1317 (2010).
[45] F.S. Delgado, J. Sanchiz, C. Ruiz-Pérez, F. Lloret, M. Julve. *Cryst. Eng. Comm.*, **6**, 443 (2004).
[46] B.L. Solomon, C.P. Landee, M.M. Turnbull, J.L. Wikaira. *J. Coord. Chem.*, **67**, 3953 (2014).
[47] Q.-R. Cheng, P. Li, H. Zhou, Z.-Q. Pan, Z.-G. Xu, G.-Y. Liao, J.-Z. Chen. *J. Coord. Chem.*, **67**, 1584 (2014).
[48] Y. Wu, Y. Mu, L. Bai, S. Guo, J. Zhao, D. Li. *J. Coord. Chem.*, **67**, 1629 (2014).
[49] M. Das, B.K. Shaw, B.N. Ghosh, K. Rissanen, S.K. Saha, S. Chattopadhyay. *J. Coord. Chem.*, **68**, 1361 (2015).
[50] Z. Lin, S. Chen, Z. Lai, Y. Wang, S. Yang. *J. Coord. Chem.*, **68**, 2121 (2015).
[51] B.J.M.L. Leite Ferreira, P. Brandão, A.M. Dos Santos, Z. Gai, C. Cruz, M.S. Reis, T.M. Santos, V. Félix. *J. Coord. Chem.*, **68**, 2770 (2015).